URL: http://dx.doi.org/10.1117/12.824375

Theoretical evaluation of MTF and charge collection efficiency in CCD and CMOS image sensors

Ibrahima Djité[abc]. Pierre Magnan[a]. Magali Estribeau[a]. Guy Rolland[b]. Sophie Petit[b]. Olivier Saint-pé[c].

[a]Université de Toulouse, ISAE, 10 avenue E. Belin, 31055, Toulouse, France

[b]CNES, 18 avenue E. Belin, 31401, Toulouse, France

[c]EADS Astrium, 31 avenue des cosmonautes, 31402, Toulouse, France

ABSTRACT

Classical models used to calculate the Modulation Transfer function (MTF) of a solid-state image sensor generally use a sinusoidal type of illumination. The approach, described in this paper, consists in considering a point-source illumination to built a theoretical three-dimensional model of the diffusion and the collection of photo-carriers created within the image sensor array. Fourier transform formalism is used for this type of illumination. Solutions allow to evaluate the spatial repartition of the charge density collected in the space charge region, i.e. to get the Pixel Response Function (PRF) formulation. PRF enables to calculate analytically both MTF and crosstalk at every needed wavelengths. The model can take into account a uniformly doped substrate and an epitaxial layer grown on a highly doped substrate. The built-in electric field induced by the EPI/Substrate doping gradient is also taken into account. For these configurations, MTF, charge collection efficiency and crosstalk proportion are calculated. The study is established in the case of photodiode pixel but it can be easily extended to pinned photodiode pixels and photogate pixels.

Keywords: CMOS Image Sensor (CIS), Charge Coupled Device (CCD), Active Pixel Sensor (APS), Modulation Transfer Function (MTF) , Crosstalk, Point Spread Function(PSF), Charge collection efficiency, High/Low junction.

1. INTRODUCTION

Nowadays the solid-state image sensor world is dominated by two sorts of devices: Charge Coupled Devices (CCD) and CMOS Image Sensors (CIS). The CCD has been the dominant technology of visible photon detection and image capture over the last two decades. But thanks to the evolution of CMOS technologies, CIS devices have become an inevitable candidate for imaging applications.

Charge collection efficiency and Modulation Transfer Function (MTF) are the two main factors which give

informations about electro-optic performances of a solid-state image sensor. Charge collection efficiency also named the Internal Quantum Efficiency (IQE), gives informations about the sensivity of solid-state imagers. It represents the ratio between incoming photon number which interacts with silicon and charge collected within the space charge regions. MTF expresses the loss of contrast due to the increase of the spatial frequency. It gives informations on the image quality. The overall MTF of a solid-state image sensor can be separated into two contributions.

– Geometrical MTF[1], which is defined by the well-known expression $\sin(\pi \cdot k \cdot a)/(\pi \cdot k \cdot a)$ where a is the pixel optical aperture and k the spatial frequency.

– Diffusion MTF resulting from Crosstalk phenomena. Crosstalk is the result of the charge carriers lateral diffusion within the body of the solid-state detector. It can be formulated as the ratio between the photon number arriving on a given pixel and the charge collected by the neighboring pixels.

An additional MTF can be incorporated in the detector overall MTF, called the Sampling MTF[2]. It results from the sampling aspect of the detector array made up of rows and columns of pixels. It depends on the pixel pitch.

Models used to calculate the MTF of CCD and CIS devices generally solve the steady-state diffusion equation in the case of a sinusoidal illumination. A first model, based on the fundamental approach of Crowell and Labuda[3], have been investigated by Seib[4]. Seib's model calculates the MTF and the IQE expressions of a full frame CCD built on a uniformly doped substrate. Another model for MTF and IQE calculations largely inspired by Seib's approach has been proposed by Blouke[5] and Stevens[6,7]. They established the MTF expression of an image sensor device built on an lightly-doped epitaxial layer(or EPI layer).

These models were applied to case of full frame CCD and had taken several hypotheses which are no longer applicable in the new generations of solid-state image sensor like CIS or buried-channel interline CCD. Another major drawback of these models is the difficulty to evaluate the crosstalk proportion. This paper try to bring solutions on these needs by building a new model with lesser hypotheses and which allows both to evaluate crosstalk proportion and to make more accurate predictions on the image sensor electro-optical performances.

The model described here solves the steady-state diffusion equation in the case of a point-source illumination. Fourier Transform formalism is used to solve this equation in the detector array, to get the PRF. This parameter is defined as the signal detected by a single pixel when it is illuminated by an infinitesimally small spot of light. It allows to evaluate theoretically the overall MTF, the IQE and the crosstalk proportion. The model is applied to the case of photodiode pixel. Calculations do not take into account the optical crosstalk caused by multiple reflections on the top layer oxide stacks, and the sampling MTF is taken equal to 1 at all spatial frequencies.

In section 2, at first the theoretical approach based on point-source illumination is presented. Then overall

MTF and IQE expressions of a front-side-illuminated device are calculated. And finally the crosstalk analytical expression is given in the case of uniformly doped substrate.

In section 3, theoretical results of MTF, IQE and crosstalk are discussed, predictions on the effects of photodiode junction depth on the MTF and IQE are made. Then Crosstalk versus the substrate doping concentration is explored. And finally the MTF model is compared to MTF measurements realized on a $7\mu m$ pitch CIS manufactured in Deep Submicron Process (DSP).

2. MODEL

Theoretical calculations of MTF and charge collection efficiency of a full frame CCD image sensor have been performed by Blouke [5] and Stevens [6,7], based on the model developed by Seib [4] for an infinitely thick and uniformly doped full frame CCD image sensor . The model calculates the IQE and the MTF degradation due to diffusion spreading in the case of image sensor built on an epitaxial (EPI) material.

The solid-state image sensor used in this study is formed by photodiode pixels with a N diffusion junction built on a P-type EPI layer which is grown on a P-type highly-doped substrate. A realistic model of the EPI layer and substrate doping profile is considered. Figure (1b) shows P-type EPI layer and substrate doping profile measured thanks to SIMS measurements done on a CIS manufactured in DSP. The substrate thickness is limited to z_s as shown in figure (2). The EPI layer is characterized by a thickness z_{epi}, a doping concentration N_e, and electrons diffusion length L_e, the substrate is characterized by a different doping concentration N_s and diffusion length L_s. The N region is characterized by a junction depth z_{diff} a doping concentration N_d and diffusion length L_p. The space charge regions penetrate the N region and the EPI region to the depth z_n and z_d respectively. The space charge region lateral expansion is controlled thanks to the P-type implant P_{well}. In followings calculations a three-dimension geometry has been considered. Square pixels with a sensitive area $S = a \cdot b$ and pixel pitch p is assumed. a and b are the sensitive area width along the x and y direction respectively. This image sensor is illuminated with an infinitesimally spot of light symbolized by a Dirac $\delta(x, y)$ distribution. Due to the illumination type and the high value of P_{well}, the diffusion occurring in the spaces between two consecutive space charge regions is negligible. In the case of point-source illumination, MTF is directly given by the normalized Fourier Transform ($FT[]$) of the PRF expression:

$$MTF(k_x, k_y) = \frac{|FT[PRF(x,y)]|}{|FT[PRF(x,y)]_{k_x,k_y=0}|} = \frac{|PRF(k_x,k_y)|}{|PRF(k_x,k_y)_{k_x,k_y=0}|} \tag{1}$$

k_x and k_y are the spatial frequencies in x and y direction respectively. The PRF expression is given by the sum of current densities in each region:

$$PRF(x,y) = D_p \frac{\partial p(x,y,z)}{\partial z}|_{z=z_n} + D_e \frac{\partial n_e(x,y,z)}{\partial z}|_{z=z_d} + \int_{z_n}^{z_d} G(x,y,z)dz \tag{2}$$

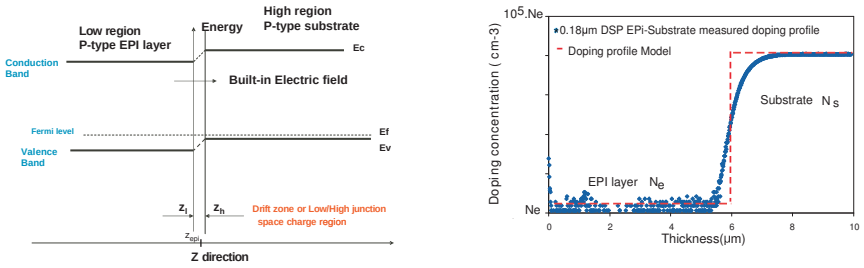

(a) **(b)**

Figure 1: Figure(1a): Low/High junction Band energy diagram. Figure(1b): SIMS measurement of a $0.18\mu m$ technology of EPI/Substrate layer and Doping profile model used for calculations

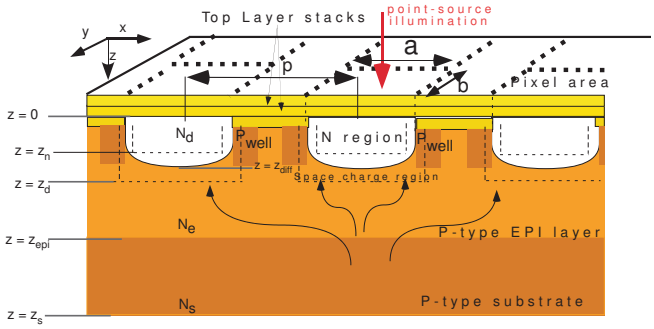

Figure 2: Geometry model used for calculations

D_p and D_e are diffusion constants for holes in the N region and for electrons in the EPI layer respectively. $p(x, y, z)$ is the excess hole concentration in the N region and $n_e(x, y, z)$ is the excess electron concentration in the EPI layer due to optical excitation. $G(x, y, z)$ is generation rate. Its expression is given thanks to the Beer Lambert's law [8]:

$$G(x, y, z) = \phi(\lambda) \cdot \alpha(\lambda) \cdot T(\lambda) \cdot exp(-\alpha z) \cdot \delta(x, y) \tag{3}$$

ϕ is the incoming photon flux at the wavelength λ, $T(\lambda)$ the transmission coefficient of top layer oxide stacks and α is the silicon absorption coefficient at λ.

The density of excess photo-generated carriers in each region is obtained by solving the steady-state diffusion equation.

Assuming that the doping profile in the N region is approximately uniform and there is no built-in electric field due to doping gradient in this region, the excess hole concentration obeys to the following equation:

$$-D_p \nabla^2 p(x, y, z) + \frac{p(x, y, z)}{\tau_p} = \phi_0 \cdot \alpha \cdot exp(-\alpha z) \cdot \delta(x, y) \tag{4}$$

$\phi_0 = \phi \cdot T(\lambda)$ is the incoming photon flux that interact directly with the silicon. This equation is subject to the boundary conditions

- $D_p \cdot \frac{\partial p(x,y,z)}{\partial z}|_{z=0} = S_p \cdot p(x,y,z)|_{z=0}$ (4.a)
- $p(x,y,z)|_{z=z_n} = 0$ (4.b)

Where S_p is the surface recombination velocity at the Silicon/Oxide interface. In the P-type EPI layer and in the substrate, the excess electron concentration are the solutions of the two following equations.

$$-D_e\nabla^2 n_e(x,y,z) + \frac{n_e(x,y,z)}{\tau_e} = \phi_0 \cdot \alpha \cdot exp(-\alpha z) \cdot \delta(x,y) \tag{5}$$

$$-D_s\nabla^2 n_s(x,y,z) + \frac{n_s(x,y,z)}{\tau_s} = \phi_0 \cdot \alpha \cdot exp(-\alpha z) \cdot \delta(x,y) \tag{6}$$

which are subject to the boundary conditions:

- $n_e(x,y,z)|_{z=z_d} = 0.$ (6.a)
- $n_s(x,y,z)|_{z=z_s} = 0.$ (6.b)
- $n_e(x,y,z)|_{z=z_{epi}} = \frac{N_s}{N_e} n_s(x,y,z)|_{z=z_{epi}}.$ (6.c)
- $qD_e \cdot \frac{\partial n_e(x,y,z)}{\partial z}|_{z=z_{epi}} = qD_s \cdot \frac{\partial n_s(x,y,z)}{\partial z}|_{z=z_{epi}} + q \cdot v_{drift} \cdot n_s(x,y,z)|_{z=z_{epi}}.$ (6.d)

$n_e(x,y,z)$ and $n_s(x,y,z)$ are the excess electron concentration in the EPI layer and in the substrate respectively. Conditions (4.b) and (6.a) simply demand that any carrier that reaches the space charge region is collected in that particular pixel. Furthermore assumption is made that there is no lateral diffusion within the space charge region.

Conditions (6.c) and (6.d) concern the EPI/substrate junction Low/High junction at $z = z_{epi}$. Low/High junctions behavior has been largely studied by Gunn [9]. Gunn has proven that in a Low/High junction, there is a creation of a drift zone as shown in figure (1a). This drift zone acts like a space charge region in which, recombination processes are neglected. In equilibrium and in the low injection conditions, the voltage across this space charge region is given by the following expression [10]:

$$V_{hl} = \frac{k \cdot T}{q} \cdot \ln(\frac{N_s}{N_e}) \tag{7}$$

k is Boltzmann constant T is detector array temperature.

Assuming that the change in minority carriers Fermi level is negligible across the junction gives:

$$n_s(x,y,z_h) = n_e(x,y,z_l) \cdot exp(-\frac{qV_{hl}}{kT}) \tag{8}$$

z_h and z_l are the drift zone extension into High and Low region respectively. A final parameter characterizing the Low/High junction is the built-in electric field $\mathcal{E}_{hl}$ created within the drift zone. In thermodynamic equilibrium, the mean value of this electric field can be formulated by:

$$\mathcal{E}_{hl} = \frac{V_{hl}}{z_h - z_l} \tag{9}$$

The drift velocity resulting from this expression is given by:

$$V_{drift} = \mu_e \cdot \mathcal{E}_{hl} \tag{10}$$

μ_e is the electron mobility in the EPI layer. This drift velocity is also named junction leakage velocity[9],[10]. It represents the minimal transport velocity with which excess minority carrier are able to cross the Low/High junction. The condition (6.c) relates the Low/High junction reflecting properties; in this case the space charge region width is not taken into account. Condition (6.d) supposes that any carrier which arrives at junction interface is drifted by the electric field to the EPI layer. Optical generation within this drift zone is also neglected. To find solution of equations (4), (5), and (6). Fourier transforms can be used. Let's take $\hat{p}(k_x, k_y, z)$, $\hat{n}_e(k_x, k_y, z)$, $\hat{n}_s(k_x, k_y, z)$, to be the bi-dimensional Fourier Transform of $p(x, y, z)$, $n_e(x, y, z)$, $n_s(x, y, z)$, respectively. These functions are the solution of the following equations:

$$-\frac{\partial^2 \hat{p}(k_x, k_y, z)}{\partial^2 z} + \frac{\hat{p}(k_x, k_y, z)}{Lk_p^2} = \frac{\phi_0 \cdot \alpha \cdot exp(-\alpha z)}{D_p} \tag{11}$$

$$-\frac{\partial^2 \hat{n}_e(k_x, k_y, z)}{\partial^2 z} + \frac{\hat{n}_e(k_x, k_y, z)}{Lk_e^2} = \frac{\phi_0 \cdot \alpha \cdot exp(-\alpha z)}{D_e} \tag{12}$$

$$-\frac{\partial^2 \hat{n}_s(k_x, k_y, z)}{\partial^2 z} + \frac{\hat{n}_s(k_x, k_y, z)}{Lk_s^2} = \frac{\phi_0 \cdot \alpha \cdot exp(-\alpha z)}{D_s} \tag{13}$$

Where $\frac{1}{Lk_i^2} = \frac{1}{L_i^2} + (2\pi k_x)^2 + (2\pi k_y)^2, i = (p, e, s)$. $L_i = \sqrt{D_i \cdot \tau_i}$ is the excess carrier diffusion length in each region. Equations (11), (12), (13) result from the Fourier Transform of equations (4), (5) and (6) respectively. The use of Fourier formalism makes easy to get MTF expression. Solutions of these equations subject to the boundary conditions (4.a),(4.b),(6.a),(6.b),(6.c),(6.d) are given by:

$$\hat{p}(k_x, k_y, z) = A_p exp(-z/Lk_p) + B_p exp(z/Lk_p) + \frac{\phi_0 \cdot \alpha \cdot exp(-\alpha z)}{D_p(\frac{1}{Lk_p^2} - \alpha^2)} \tag{14}$$

$$\hat{n}_e(k_x, k_y, z) = A_e exp(-z/Lk_e) + B_e exp(z/Lk_e) + \frac{\phi_0 \cdot \alpha \cdot exp(-\alpha z)}{D_e(\frac{1}{Lk_e^2} - \alpha^2)} \tag{15}$$

$$\hat{n}_s(k_x, k_y, z) = A_s exp(-z/Lk_s) + B_s exp(z/Lk_s) + \frac{\phi_0 \cdot \alpha \cdot exp(-\alpha z)}{D_s(\frac{1}{Lk_s^2} - \alpha^2)} \tag{16}$$

with $\frac{1}{Lk_i} \neq \alpha$.

A_i and $B_i, (i = p, e, s)$ expressions are given in Appendix A. From these expressions, $PRF(k_x, k_y)$ can be derived using relations (1) and (2), and the $MTF(k_x, k_y)$ expression is directly obtained.

$$MTF(k_x, k_y) = \frac{M_p(k_x, k_y) + M_e(k_x, k_y) + \phi_0(e^{-\alpha z_n} - e^{-\alpha z_d}) sinc(\pi k_x \cdot x_p) \cdot sinc(\pi k_y \cdot y_p)}{M_p(0,0) + M_e(0,0) + \phi_0(e^{-\alpha z_n} - e^{-\alpha z_d})} \tag{17}$$

Expressions of $M_p(k_x, k_y)$ and $M_e(k_x, k_y)$ are given in the Appendix A. The charge collection efficiency is given by:

$$IQE = \frac{(\frac{D_e}{L_e}(-A_e e^{-\frac{z_d}{L_e}} + B_e e^{\frac{z_d}{L_e}} - \alpha\gamma_e e^{-\alpha z_d}) - \frac{D_p}{L_p}(-A_p e^{-\frac{z_n}{L_p}} + B_p e^{\frac{z_n}{L_p}} - \alpha\gamma_p e^{-\alpha z_n}) + \phi_0(e^{-\alpha z_n} - e^{-\alpha z_d}))}{\phi_0} \tag{18}$$

γ_i (i=e,p) is given in Appendix. Note that with taking $N_s = N_e$ gives MTF and IQE expressions in the case of uniformly doped substrate. crosstalk expression is derived directly from PRF(x,y) expression. Assuming there is no lateral diffusion in the N region, the crosstalk is directly given by the inverse Fourier transform of $M_e(k_x, k_y)$ which represent the EPI/Substrate contribution. Crosstalk expression is calculated thanks to the Complex formalism which allows to find the inverse Fourier transform of $M_e(k_x, k_y)$. Crosstalk analytical expression on x direction as defined sooner is given when $N_s = N_e$ by.

$$crosstalk(\lambda) = \frac{L_e}{(z_s - z_d)} \sum_{n=1}^{+\infty} \frac{(1 + (-1)^{n+1} exp(-\alpha(z_s - z_d))) exp(\frac{-a}{2L_e\sqrt{1+(\frac{n\pi L_e}{z_s - z_d})^2}})}{((1 + (\frac{\alpha*(z_s - z_d)}{n\pi})^2)(1 + (\frac{n\pi L_e}{z_s - z_d})^2))} \tag{19}$$

The crosstalk expression on y direction is easily obtained by replacing a by b in the previous the expression.

3. RESULTS

Figures (3) present the overall MTF calculations of a solid state image sensor built on a EPI layer. The overall MTF is plotted at different values of λ. The device is assumed to have $p = 7\mu m$ pixel pitch and a thickness z_s. The N region is assumed to have a constant doping profile with a doping concentration $N_d \approx 10^{17} cm^{-3}$ a width a and b along x and y directions respectively such as $\frac{a}{b} \approx 0.86$. The EPI layer is characterized by a doping density N_e and a thickness z_{epi}. The substrate is assumed to be highly doped with a doping density N_s such as $\frac{N_s}{N_e} \approx 10^4$. Carriers diffusion constants, lifetimes, and diffusion lengths in each of these regions have been calculated thanks to the empiric relations established by Taur [11], Swirhun [12, 13], and Alamo [14, 15]. Figures (3a) and (3b) represent the MTF as the function of spatial frequency along x and y directions respectively for a given value of junction depth. For short wavelengths ($\lambda < 0.5\mu m$) the carriers are generated in the N region near the surface $z = 0$ so the contribution of EPI layer is small. The overall MTF approaches the expression $MTF(k_x, k_y) \approx \frac{M_p(k_x, k_y)}{M_p(0,0)}$ and is largely influenced by the N regions physical characteristics. For

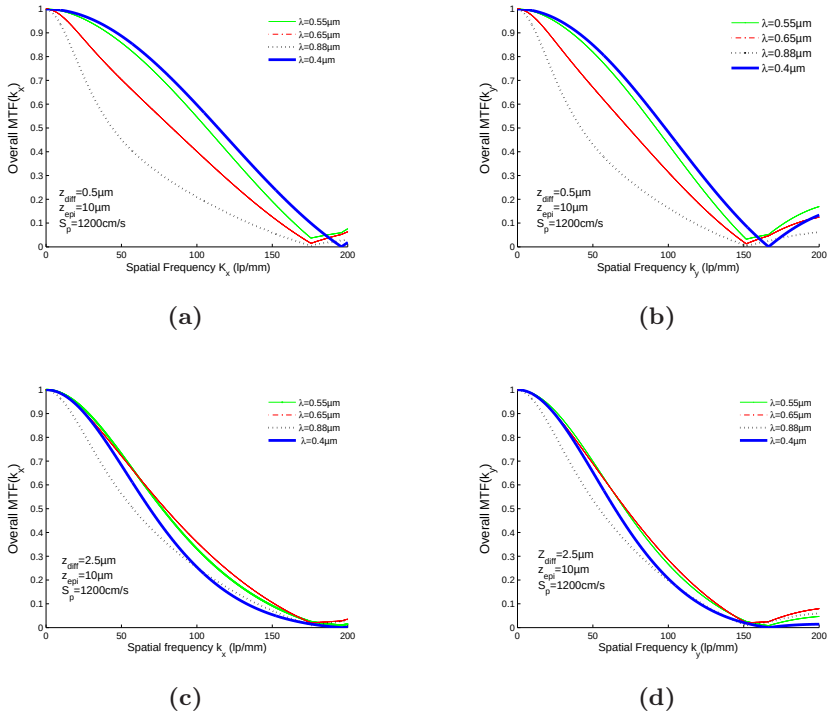

Figure 3: Figures (3a) and (3b) plot respectively the horizontal and vertical overall MTF of a shallow junction-depth ($z_{diff} = 0.5\mu m$) photodiode pixel. Figures (3c) and (3d) plot those of deep junction-depth ($z_{diff} = 2.5\mu m$)

large wavelengths ($\lambda > 0.680\mu m$) carriers are generated deeply in the EPI layer and in the substrate. The overall MTF approaches the expression $\frac{M_e(k_x,k_y)}{M_e(0,0)}$ and is largely dominated by the diffusion contribution of the EPI layer. For wavelengths between ($0.50\mu m < \lambda < 0.650\mu m$) the generation within the space charge region become the dominated contribution and so the overall MTF is mostly influenced by geometrical MTF contribution. Overall MTF is also plotted at different values of photodiode junction depth z_{diff}. For shallow junction depth (i.e $z_{diff} \leq 0.5\mu m$),at Nyquist frequency $k_i = \frac{1}{2p}$, the overall MTF have greater values for short wavelengths and then decreases when λ becomes large. For deep junction depth (i.e $z_{diff} \geq 1.4\mu m$), the overall MTF greatest values at Nyquist frequency are obtained for $0.5\mu m < \lambda < 0.68\mu m$. These results can be easily applied to N_{well}-type photodiode pixel which have deeper junction depth than N_{cis}-type photodiode pixel.

Figure (4a) represents the evolution of IQE as the function of wavelength. The study is done using a realistic value of surface recombination velocity S_p [16] at silicon/oxide interfaces. This figure compares the IQE of a solid-state imager built on a uniformly and lightly doped substrate (i.e $\frac{N_s}{N_e} = 1$ and value of N_e is not changed), and another one built on lightly doped EPI layer grown on highly doped substrate. The value of IQE of uniformly doped substrate is greater than those built on EPI layer for large wavelengths. On the other side, figure (4b) shows that overall MTF of solid state imager built on EPI layer, is greater than those built on uniformly and

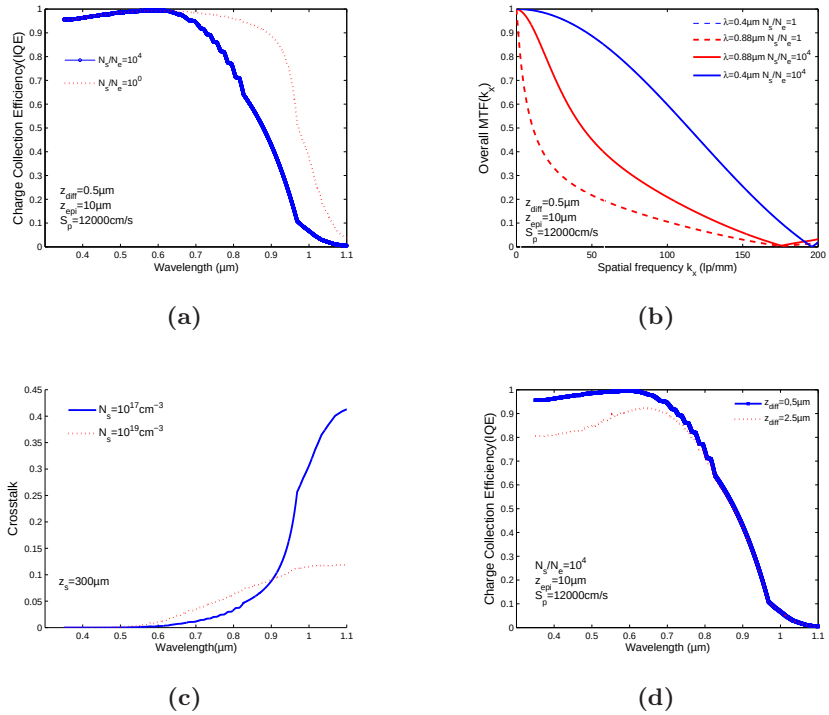

Figure 4: Figures (4a) and (4b) compare the IQE and MTF at two values of $\frac{N_s}{N_e}$ and Figure (4d) plots IQE at two values of junction depth of a photodiode pixel. Figure (4c) plots the crosstalk for two values of doping concentration

lightly-doped substrate for large wavelengths. The conclusion of that is a trade-off must be found between needs into image quality and sensivity. Recent works are trying to improve sensivity at the large wavelengths without degrading the overall MTF. These works are focused on increasing the drift contribution by using complex doping profile to drift photo-carriers toward space charge regions [17]. Crosstalk proportion is also plotted in figure (4c) at different values of substrate doping concentration. Note that changing the doping concentration have the same consequence that changing the photodiode junction depth (i.e changing substrate doping concentration or photodiode junction depth will change the space charge region extension) on the results on crosstalk proportion . The crosstalk have its greatest value at large wavelengths and increase when the substrate becomes lightly doped. This effect have induced the decrease of overall MTF value shown on figure (4b) when $\frac{N_s}{N_e} = 1$. The results of Figure(4d) show that the IQE of a shallow junction depth photodiode pixel is nearly an order of magnitude higher than those of deep junction depth photodiode at short wavelengths. This results can be explained by the impact of the surface recombination velocity S_p in the IQE. This impact is indeed more significative on deep junction depth than on shallow junction depth photodiode pixel. Note that with taking a lower value of S_p gives approximately the same value of IQE for both configurations.

The overall MTF calculations have been also confronted with experimental measurements realized on a $7\mu m$

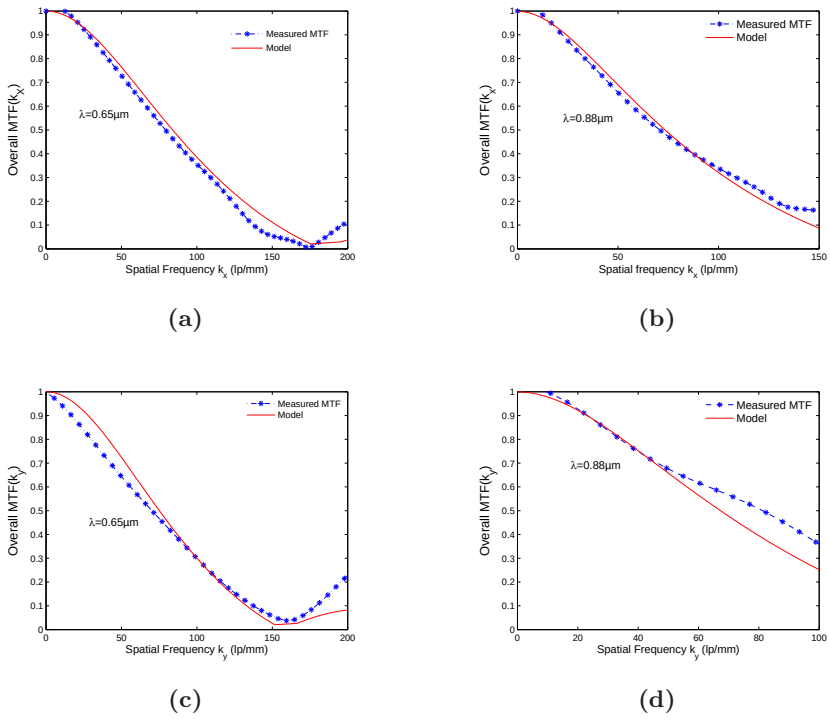

Figure 5: Overall MTF model and Measured MTF versus wavelength in x =horizontal and y =vertical directions

pitch CIS manufactured in $0.18\mu m$ technology as shown in figure (5). Thanks to the measurement methods that allow to align with accuracy the target and the detector array, the phasing effects are, in this case, canceled and the sampling MTF is practically equal to 1 at all spatial frequencies. Therefore the measured MTF can be compared with the model established above. The model fits well the measured MTF with taking realistic values of S_p: $650cm/s < S_p < 12000cm/s$ and values of z_{diff} between $1.4\mu m < z_{diff} < 2.6\mu m$.

4. CONCLUSIONS

Theoretical expressions of MTF charge collection efficiency and crosstalk proportion have been evaluated using point-source illumination. The advantage of this model over numerical approaches (i.e physical simulations with SENTAURUS) is that of speed. The numerical approach can take hours of execution times, whereas the analytical expressions once modeled, can be easily and quickly used for making predictions. Predictions have been made on the electro-optics performances versus the image sensor physical characteristics. The theoretical results of overall MTF are confronted with experimental measurements. Confrontations shows that models established present very good estimate at large wavelengths in the scale of spatial frequencies from 0 to Nyquist frequency. Short wavelengths ($\lambda < 0.4\mu m$) are not studied in the case of this article, the study of these scales of wavelengths needs a good knowledge of surface recombination processes at oxide silicon interfaces and optical

crosstalk which can play an important role on the electro-optics performances at short wavelengths of visible spectrum. Future works will be focused on extending the crosstalk expression to the case of image sensor built on the EPI/substrate configuration.

5. ACKNOWLEDGMENTS

The authors are grateful to Paola Cervantès (ISAE), for her work on MTF measurements and to Florie Mialhe (CNES) for her help on SIMS measurements. Vincent Goiffon is thanked for his help on SIMS data analysis. We also thank Franck corbière, Sébastien Rolando and Cedric Virmontois (ISAE) for discussions held about image sensor geometrical characteristics. Thanks to CNES and EADS-Astrium for their financial and technical support.

REFERENCES

[1] Yadid-Pecht, O., "Geometrical modulation transfer function for different pixel active area shapes," *Optical Engineering* **39**, 859–865 (Apr. 2000).

[2] Park, S., Schowengerdt, R., and Kaczynski, M., "Modulation-transfer-function analysis for sampled image systems," *Applied optics* **23**(15), 2572–2582 (1984).

[3] Crowell, M. H. and Labuda, E. F., "The silicon diode array camera tube," *Bell Syst. Tech.J* **48**, 1481–128 (1969).

[4] Seib, D., "Carrier diffusion degradation of modulation transfer function in charge coupled imagers," *Electron Devices, IEEE Transactions on* **21**(3), 210–217 (1974).

[5] Blouke, M. and Robinson, D., "A method for improving the spatial resolution of frontside-illuminated ccd's," *Electron Devices, IEEE Transactions on* **28**(3), 251–256 (Mar 1981).

[6] Stevens, E., "A unified model of carrier diffusion and sampling aperture effects on mtf in solid-state image sensors," *Electron Devices, IEEE Transactions on* **39**(11), 2621–2623 (Nov 1992).

[7] Stevens, E. and Lavine, J., "An analytical, aperture, and two-layer carrier diffusion mtf and quantum efficiency model for solid-state image sensors," *Electron Devices, IEEE Transactions on* **41**(10), 1753–1760 (1994).

[8] Bouguer, P., [*Essai d'optique sur la gradation de la lumire*] (1729).

[9] Gunn, J. B., "On carrier accumulation, and the properties of certain semiconductor junctions," *International Journal of Electronics* **4**(1), 17 – 50 (1958).

[10] Hauser, J., "Minority carrier reflecting properties of semiconductor high-low junctions," *Solid State Electronics* **18**, 715–716 (Aug. 1975).

[11] Taur, Y. and Ning, T. H., [*Fundamentals of MODERN VLSI DEVICES*], The Press Syndicate Of The University Of Cambridge (1998).

[12] Swirhun, S., Kwark, Y.-H., and Swanson, R., "Measurement of electron lifetime, electron mobility and band-gap narrowing in heavily doped p-type silicon," *Electron Devices Meeting, 1986 International* **32**, 24–27 (1986).

[13] Swirhun, S., del Alamo, J., and Swanson, R., "Measurement of hole mobility in heavily doped n-type silicon," *Electron Device Letters, IEEE* **7**, 168–171 (Mar 1986).

[14] del Alamo, J. and Swanson, R., "The physics and modeling of heavily doped emitters," *Electron Devices, IEEE Transactions on* **31**, 1878–1888 (Dec 1984).

[15] del Alamo, J., Swirhun, S., and Swanson, R., "Simultaneous measurement of hole lifetime, hole mobility and bandgap narrowing in heavily doped n-type silicon," *Electron Devices Meeting, 1985 International* **31**, 290–293 (1985).

[16] Lin, C.-S., Mathur, B., and Chang, M.-C., "Analytical charge collection and mtf model for photodiode-based cmos imagers," *Electron Devices, IEEE Transactions on* **49**(5), 754–761 (2002).

[17] Bogaerts, J., De Moor, P., De Munck, K., Tezcan, D., and Van Hoof, C., "DEVELOPMENT OF CMOS ACTIVE PIXEL SENSORS FOR EARTH OBSERVATION," **1** (2007).

APPENDIX A.

$$B_p = \frac{\frac{\phi_0\alpha}{-D_p(\alpha^2-\frac{1}{Lk_p^2})}(D_p\alpha+S_p-(\frac{D_p}{Lk_p}+S_p)exp(-\alpha z_n+\frac{z_n}{Lk_p}))}{\frac{D_p}{Lk_p}-S_p+(\frac{D_p}{Lk_p}+S_p)exp(\frac{2z_n}{Lk_p})};\ A_p = -B_p exp(\frac{2z_n}{Lk_p}) - \frac{\phi_0\alpha}{-D_p(\alpha^2-\frac{1}{Lk_p{}^2})}exp(-\alpha z_n+\frac{z_n}{Lk_p})$$

$$\gamma_i = -\frac{\phi_0\alpha}{D_i(\alpha^2-\frac{1}{Lk_i^2})};\ \gamma_s = -\frac{\phi_0\alpha}{D_s(\alpha^2-\frac{1}{Lk_s^2})};\ const_0 = \frac{exp(\frac{zs}{Lk_s}-\frac{z_d}{Lk_e})sinh(\frac{zepi-zs}{Lk_s})}{sinh(\frac{z^d-z_{epi}}{Lk_e})};$$

$$const_1 = \frac{2\gamma_e(exp((-\alpha+\frac{1}{Lk_e})\frac{z_d+z_{epi}}{2})sinh((\frac{1}{Lk_e}-\alpha)\frac{z_{epi}-z_d}{2}))+\gamma_s\frac{N_s}{N_e}(-exp(-\alpha z_s+\frac{z_s}{Lk_s}-\frac{z_{epi}}{Lk_s}+\frac{z_{epi}}{Lk_e})+exp(-\alpha zepi+\frac{zepi}{Lk_e}))}{2exp(\frac{zd+zepi}{Lk_e})sinh(\frac{z_d-z_{epi}}{Lk_e})}$$

$$term_{10} = \gamma_e exp(-\alpha z_d+\frac{z_d}{Lk_e}-\frac{z_{epi}}{Lk_e});\ term_{11} = \gamma_s exp(-\alpha z_s+\frac{z_s}{Lk_s}-\frac{z_{epi}}{Lk_s});\ term_{20} = 2exp(\frac{z_d}{Lk_e})cosh(\frac{z_{epi}-z_d}{Lk_e});$$

$$term_{30} = 2exp(\frac{z_s}{Lk_s})cosh(\frac{zs-zepi}{Lk_s});\ term_{40} = 2exp(\frac{z_s}{Lk_s})sinh(\frac{zepi-zs}{Lk_s});\ term_{41} = \gamma_s(exp(-\alpha z_{epi}) - exp(-\alpha z_s+$$

$$\frac{z_s}{Lk_s}-\frac{z_{epi}}{Lk_s}));\ B_s = \frac{\frac{D_e}{Lk_e}(term_{10}+const_1 term_{20})-\frac{D_s}{Lk_s}term_{11}-V_{drift}term_{41}}{-\frac{N_s}{N_e}\frac{D_e}{Lk_e}const_0 term_{20}+\frac{D_s}{Lk_s}term_{30}+V_{drift}term_{40}};\ B_e = B_s\frac{N_s}{N_e}const_0+const_1;\ A_s = -\gamma_s exp(-\alpha z_s+$$

$$+\frac{z_s}{Lk_s}) - B_s exp(\frac{2z_s}{Lk_s});\ A_e = -\gamma_e exp(-\alpha z_d+\frac{z_d}{Lk_e}) - B_e exp(\frac{2z_d}{Lk_e})$$

$$M_p(k_x,k_y) = \frac{D_p}{Lk_p}(B_p e^{-\frac{z_n}{Lk_p}} - A_p e^{-\frac{z_n}{Lk_p}} + \frac{\phi_0\alpha^2 Lk_p}{D_p(\alpha^2-\frac{1}{Lk_p^2})}e^{-\alpha z_n})\cdot sinc(\pi k_x\cdot x_n)\cdot sinc(\pi k_y\cdot y_n)$$

$$M_e(k_x,k_y) = \frac{D_e}{L_{ke}}(B_e e^{-\frac{z_d}{Lk_e}} - A_e e^{-\frac{z_d}{L_{ke}}} + \frac{\phi_0\alpha^2 Lk_e}{D_e(\alpha^2-\frac{1}{L_{ke}^2})}e^{-\alpha z_d})\cdot sinc(\pi k_x\cdot x_p)\cdot sinc(\pi k_y\cdot y_p)$$

$$x_n = a-2\sqrt{\frac{2\epsilon_{si}P_{well}V_{bias}}{qN_d(P_{well}+N_d)}};\ x_p = a+2\sqrt{\frac{2\epsilon_{si}N_dV_{bias}}{qPwell(Pwell+N_d)}};\ y_n = b-2\sqrt{\frac{2\epsilon_{si}P_{well}V_{bias}}{qN_d(P_{well}+N_d)}};\ y_p = b+2\sqrt{\frac{2\epsilon_{si}N_dV_{bias}}{qPwell(P_{well}+N_d)}}$$